Impact of incomplete martensitic phase transition on the magnetic behavior of Co-doped $MnNiGe_{1.05}$ alloys

Riya Roy,[1] Sanat Kumar Adhikari,[1] Sambhu Charan Das,[1,2] Rosni Roy,[1] Sabyasachi Pramanick,[1] Kalyanashis De,[3] Oleh Ivashko,[4] Ann-Christin Dippel,[4] Martin von Zimmermann,[4] Sudipta Bandyopadhyay,[5] Rajib Mondal,[1] and Souvik Chatterjee[1,*]

[1]*UGC-DAE Consortium for Scientific Research, Kolkata Centre, Sector III, LB-8, Salt Lake, Kolkata 700 106, India*
[2]*Department of Physics, Tamkang University, New Taipei City 251301, Taiwan*
[3]*School of Science and Technology, The Neotia University, South 24 Parganas 743368, India*
[4]*Deutsches Elektronen-Synchrotron DESY, Notkestraße 85, 22607 Hamburg, Germany*
[5]*Department of Physics, University of Calcutta, 92 A.P.C. Road, Kolkata 700009, India*

(Received 2 January 2024; accepted 5 April 2024; published 23 April 2024)

Co-doped $MnNiGe_{1.05}$ alloys of nominal compositions $MnNi_{1-x}Co_xGe_{1.05}$ (for $x = 0.075$ and 0.125), with a significant amount of vacancies at the transition-metal sites, have been explored through temperature-dependent structural and magnetic investigations. Such studies confirm the presence of martensitic phase transition (MPT) in both the alloys. However, the observed MPT is found to be incomplete in nature. The presence of a significant amount of high-temperature austenite phase, well below the MPT, results in several interesting features, including field-induced metamagnetic transition and nonmonotonic change in the inverse magnetocaloric behavior, etc. In addition, a possible spin-reorientation transition has also been noticed in the magnetically ordered austenite phase for both the alloys.

DOI: 10.1103/PhysRevB.109.144420

I. INTRODUCTION

In last two decades, magnetic shape-memory alloys (MSMAs) have attracted considerable attention due to their intriguing physical/functional properties [1–10]. In MSMAs, both shape and size of the materials can be controlled, not only by the temperature (T) and stress, but also by the application of external magnetic fields (H). Though stoichiometric and off-stoichiometric Heusler alloys are the most famous examples of MSMAs, magnetic equiatomic alloys (MEAs) of general formula MM′X (M, M′ = transition metals, X = Ge, Si, Sn, etc.) have recently been identified as a new class of shape-memory alloys and gained significant importance among researchers [11–24]. Apart from the shape-memory property, MEAs are particularly important for their multiple functional properties, e.g., large magnetocaloric effect (MCE), magnetoresistance (MR), exchange bias (EB), etc. [11–24].

Among various members of MEAs, several works have been performed on pure and doped MnNiGe alloys [13–28]. Pristine MnNiGe alloy undergoes a martensitic phase transition (MPT) from high-temperature hexagonal Ni_2In-type structure (space group $P6_3/mmc$) to low-temperature orthorhombic TiNiSi-type structure (space group $Pnma$) at 470 K during cooling [12,13]. Both martensite (low-temperature phase) and austenite (high-temperature phase) phases in stoichiometric MnNiGe alloy are paramagnetic (PM) in nature around MPT. On further cooling, it orders antiferromagnetically below 346 K [12]. The main aim behind the doping studies (by perturbing different sites) is to bring the MPT below or around the magnetic transition temperatures for better magnetofunctionality [13–24]. The most common perturbation approaches are: (i) doping of smaller- or larger-sized foreign elements at different sites of the material, (ii) self-doping, (iii) vacancy creation, and (iv) application of external pressure [13–28]. Recent neutron diffraction studies reveal the strong effect of foreign-element doping on the magnetic structure of these alloys [29,30]. Depending on the doping sites, different magnetic structures have been observed, e.g., (i) cycloidally modulated incommensurate antiferromagnetic (AFM) martensite phase in Mn-site doped alloys [29], (ii) helically modulated incommensurate AFM martensite phase in Ni-site doped alloys [29], (iii) commensurate AFM austenite and helically modulated incommensurate AFM martensite phases in Ge-site doped alloys [30].

To date, several studies on the foreign-element-doped MnNiGe alloys have been performed [13–28]. However, the least-attempted one is to create vacancies at the transition-metal sites to influence the magnetic and MPT temperatures and, hence, the magnetofunctionality [14]. In the present work, we are going to focus on $MnNi_{1-x}Co_xGe_{1.05}$ (for $x = 0.075$, 0.125) alloys, where vacancy is being induced both at the Mn and Ni sites, along with the replacement of some Ni atoms by Co atoms. The main aim here is to perturb the magnetic ground state of the material and enhance its magnetofunctionality. Our investigation reveals several unique observations in these vacancy-induced alloys. Most importantly, we noticed incomplete MPT in both the alloys with a large percentage ($> 22\%$) of high-T austenite phase remains

*souvik@csr.res.in; souvikchat@gmail.com

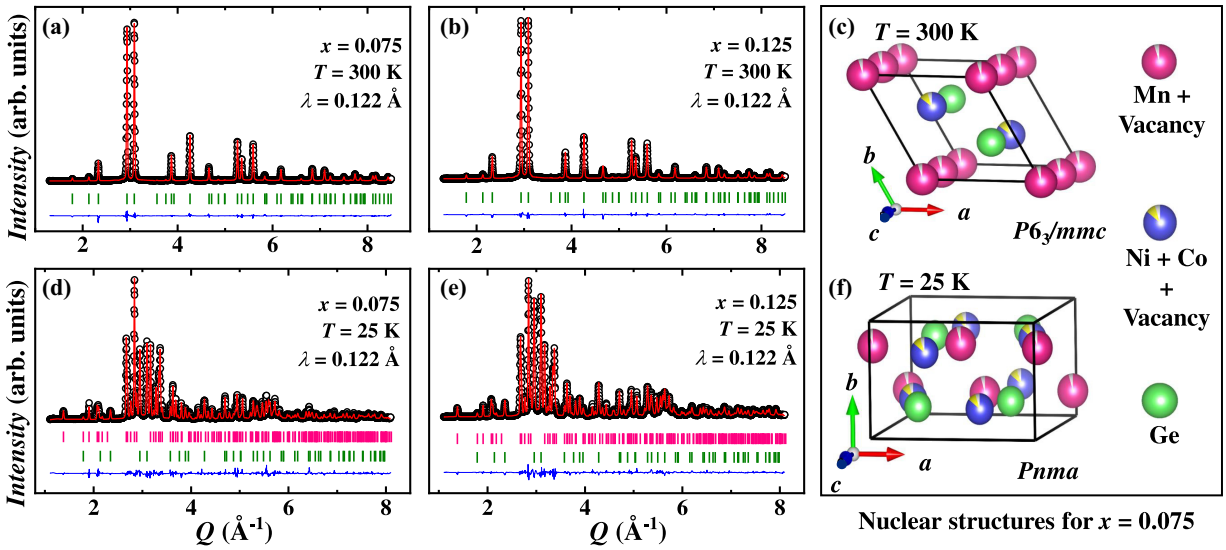

FIG. 1. X-ray powder diffraction data, recorded using P21.1 beamline of PETRA-III electron storage ring, at 300 K [(a) and (b)] and 25 K [(d) and (e)] for both the alloys are plotted. Here, black circles, red lines, and blue lines represent the observed, calculated, and difference patterns, respectively. The olive and pink vertical bars indicate the Bragg's peak position for hexagonal ($P6_3/mmc$) and orthorhombic ($Pnma$) phases, respectively. (c) and (f) depict the hexagonal (austenite) and orthorhombic (martensite) structures, respectively, of a representative alloy of composition $MnNi_{0.925}Co_{0.075}Ge_{1.05}$.

untransformed even at the lowest T of measurements. In literature, there are few examples of incomplete MPT in doped MEAs. However, the observed untransformed austenite phase was found to be significantly small ($< 15\%$) [13,29,30]. Apart from the incomplete MPT, the possible signature of spin-reorientation transition in the magnetically ordered austenite phase and the presence of large conventional and inverse MCEs are some other salient features of the presently studied alloys. Incomplete MPT triggered field-induced metamagnetic transition and nonmonotonic variation of inverse MCE in the low-T region (around the MPT).

II. EXPERIMENTAL DETAILS

The polycrystalline samples of nominal compositions $MnNi_{1-x}Co_xGe_{1.05}$ (for $x = 0.075$ and 0.125) were prepared by arc melting the constituent elements of purity $>99.9\%$ under a high-purity argon atmosphere using a Centorr-make tri-arc furnace. During melting, the electrical current was carefully controlled so that there was minimum weight loss. The alloys were remelted four times to achieve the required homogeneity. The arc-molten ingots were then sealed in an evacuated quartz capsule and annealed at 800 °C for 100 hours, followed by a quick quenching in ice water. The samples were characterized through T-dependent x-ray diffraction (XRD) measurements performed at the broad-band diffraction beamline P21.1 at the PETRA-III electron storage ring at DESY, Germany. The energy of the incident x-ray beam was selected to be $E_{photon} = 101.55$ keV (wavelength $\lambda \sim 0.122$ Å). During the diffraction measurements, the samples were mounted in kapton-make capillaries and placed on a displex cold-finger cryostat, with a T range of 10–320 K. The Rietveld refinement analysis of the recorded XRD patterns was performed using the FULLPROF software package, and the crystallographic structure of different phases was visualized through the VESTA software package [31,32]. The dc magnetization data were recorded using a vibrating sample magnetometer (VSM) from Cryogenic Ltd., UK, between 5–300 K with H range of ± 150 kOe. For better T stability, He-exchange gas was used in the sample chamber. During isothermal measurements, the observed temperature fluctuation was found to be less than 15 mK.

III. RESULTS AND DISCUSSION

A. High-energy XRD results

The XRD patterns, recorded at room T (300 K), for both the alloys, along with the refinement and difference patterns and Bragg peak positions, are plotted in Figs. 1(a) and 1(b). Both the alloys are found to possess Ni_2In-type hexagonal structure with space group $P6_3/mmc$ at room T. No additional phase has been detected in any of the alloys. Due to the presence of vacancy in both the transition-metal sites, we decided to probe the distribution of Co in both the available transition-metal sites (Mn and Ni) through Rietveld refinement analysis. We noticed small negative values of the occupancy parameters of Co for Mn site in the studied alloys. Such behavior confirms the incorporation of Co in the Ni site only, in both the Co-doped alloys. Refinement analysis also corroborates the vacancy in both Mn and Ni sites for the presently studied alloys. The hexagonal lattice parameters obtained match well with the previously reported pure and doped MnNiGe alloys [29,30]. All relevant refinement parameters are listed in Table I. The hexagonal crystal structure of one of the representative alloys, $MnNi_{0.925}Co_{0.075}Ge_{1.05}$, is shown in Fig. 1(c).

Subsequently, we reduced the sample temperature and recorded the XRD pattern at 25 K. The observed diffraction patterns are found to be significantly different from the room-T pattern. Such a change in the diffraction pattern is due to the presence of MPT in the presently studied alloys. Both the

TABLE I. Various structural parameters obtained from the Rietveld refinement of XRD data at 300 K and 25 K for $MnNi_{1-x}Co_xGe_{1.05}$ (for $x = 0.075$ and 0.125) alloys.

$MnNi_{0.925}Co_{0.075}Ge_{1.05}$						$MnNi_{0.875}Co_{0.125}Ge_{1.05}$					
$T = 300$ K: Austenite Phase - Hexagonal (Space group : $P6_3/mmc$)											
$a = 4.069(2)$ Å		$c = 5.392(1)$ Å			$\gamma = 120^\circ$	$a = 4.066(4)$ Å		$c = 5.389(3)$ Å			$\gamma = 120^\circ$
Type	Site	x	y	z	B_{iso}	Type	Site	x	y	z	B_{iso}
Mn	2a	0.000	0.000	0.000	0.510(4)	Mn	2a	0.000	0.000	0.000	0.173(3)
Ni	2d	0.333	0.666	0.750	1.021(6)	Ni	2d	0.333	0.666	0.750	1.342(5)
Co	2d	0.333	0.666	0.750	1.021(6)	Co	2d	0.333	0.666	0.750	1.342(5)
Ge	2c	0.333	0.666	0.250	0.922(5)	Ge	2c	0.333	0.666	0.250	0.910(4)
$T = 25$ K : Austenite Phase - Hexagonal (Space group : $P6_3/mmc$)											
$a = 4.060(1)$ Å		$c = 5.356(3)$ Å			$\gamma = 120^\circ$	$a = 4.059(2)$ Å		$c = 5.349(4)$ Å			$\gamma = 120^\circ$
Phase fraction = 22.81(±0.57)%						Phase fraction = 35.02(±0.37)%					
Type	Site	x	y	z	B_{iso}	Type	Site	x	y	z	B_{iso}
Mn	2a	0.000	0.000	0.000	0.150(1)	Mn	2a	0.000	0.000	0.000	1.377(2)
Ni	2d	0.333	0.666	0.750	0.943(2)	Ni	2d	0.333	0.666	0.750	2.488(1)
Co	2d	0.333	0.666	0.750	0.943(2)	Co	2d	0.333	0.666	0.750	2.488(1)
Ge	2c	0.333	0.666	0.250	0.651(2)	Ge	2c	0.333	0.666	0.250	2.218(3)
$T = 25$ K : Martensite Phase - Orthorhombic (Space group : $Pnma$)											
$a = 5.976(4)$ Å		$b = 3.733(2)$ Å		$c = 7.025(2)$ Å		$a = 5.970(3)$ Å		$b = 3.726(2)$ Å		$c = 7.017(1)$ Å	
Phase fraction = 77.19(±1.02)%						Phase fraction = 64.98(±0.54)%					
Type	Site	x	y	z	B_{iso}	Type	Site	x	y	z	B_{iso}
Mn	4c	0.025(2)	0.250	0.181(4)	0.287(3)	Mn	4c	0.025(4)	0.250	0.182(2)	0.420(5)
Ni	4c	0.150(4)	0.250	0.564(2)	0.394(1)	Ni	4c	0.148(6)	0.250	0.560(4)	0.759(1)
Co	4c	0.150(4)	0.250	0.564(2)	0.394(1)	Co	4c	0.148(6)	0.250	0.560(4)	0.759(1)
Ge	4c	0.761(3)	0.250	0.622(4)	0.637(3)	Ge	4c	0.761(4)	0.250	0.622(2)	0.563(2)

XRD patterns, recorded at 25 K, along with the refinement patterns, are depicted in Figs. 1(d) and 1(e) for $x = 0.075$ and 0.125 alloys, respectively. The refinement analysis confirms the presence of the majority of TiNiSi-type orthorhombic phase (space group *Pnma*) in the low-T region. However, the MPT is found to be incomplete in both the alloys, and a significant amount of the high-T hexagonal phase is also found to be present along with the low-T orthorhombic phase. For $x = 0.075$ and 0.125 alloys, about 22.81% (±0.57) and 35.02% (±0.37) of high-T hexagonal phase have been noticed, respectively, at 25 K. This behavior significantly differs from the pure and doped MnNiGe alloys with no vacancy [13,29,30]. All the relevant refinement parameters for both the phases at 25 K are listed in Table I. To probe the T evolution of both hexagonal and orthorhombic phases, we recorded XRD data at different constant T between 25–300 K. A restricted region of such XRD patterns is represented through the contour plot in Figs. 2(a) and 2(b) for $x = 0.075$ and 0.125 alloys, respectively. From these contour plots, we exactly determined the martensitic phase transition temperature (T_M) for the alloys (marked by a dashed line), which are 170 K and 120 K for $x = 0.075$ and 0.125 alloys, respectively. The observed T_Ms are in good agreement with the previously reported data of similar MEAs [14]. The orthorhombic peaks below the T_M are clearly visible in the contour plots for both the alloys. Such plots also confirm the existence of high-T hexagonal

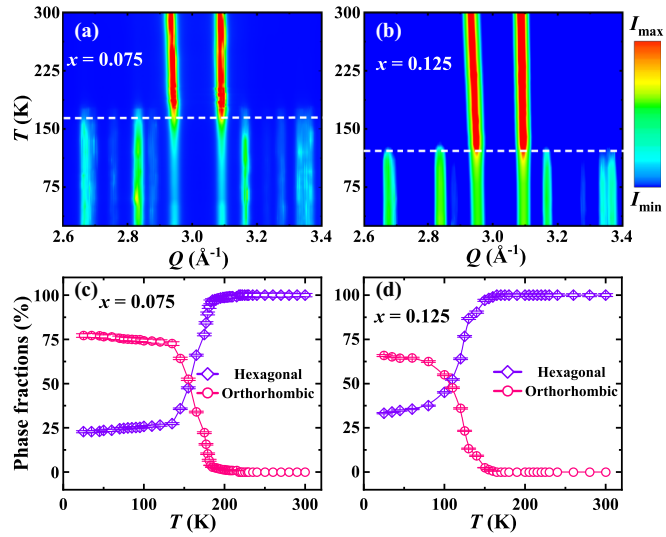

FIG. 2. Contour plots of a restricted region of the temperature evolution of the hexagonal and orthorhombic reflections are depicted in (a) and (b) for $x = 0.075$ and 0.125 alloys, respectively. The white dashed line indicates the martensitic phase transition temperature of the studied alloys. The color bar presented in the right-hand side specifies the normalized intensities. The temperature variation of the orthorhombic and hexagonal phase fractions for $x = 0.075$ and 0.125 alloys are plotted in (c) and (d), respectively.

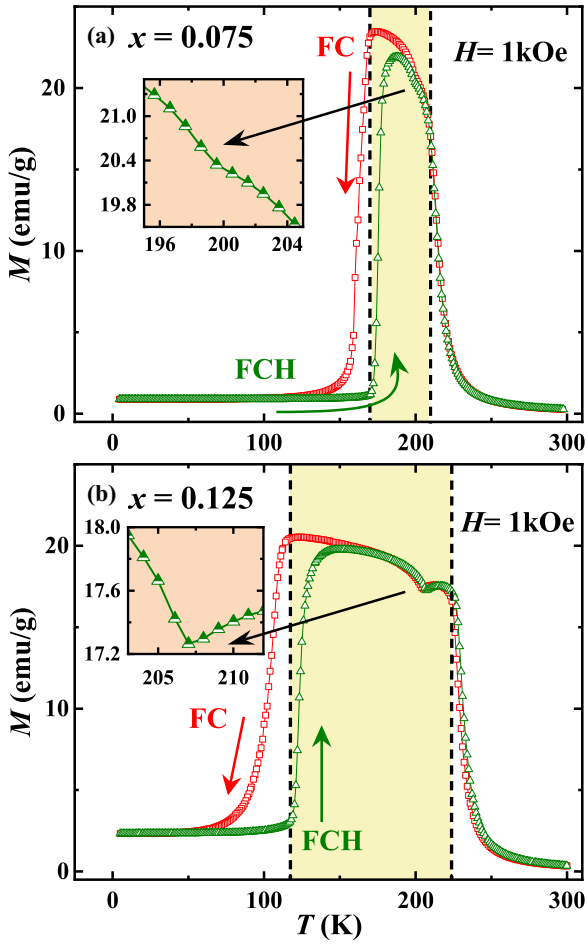

FIG. 3. Temperature variation of dc magnetization data, recorded in the presence of 1 kOe of external magnetic fields, under field cooling (FC) and field-cooled heating (FCH) protocols are depicted in the main panels of (a) and (b) for $x = 0.075$ and 0.125 alloys, respectively. Insets show the enlarged view of the anomaly observed in the magnetically ordered austenite phase.

reflections below the MPT point. From the refinement analysis of the T-dependent XRD data, we extracted the variation of both hexagonal and orthorhombic phase fractions as a function of T. T dependence of phase fractions are plotted in Figs. 2(c) and 2(d) for $x = 0.075$ and 0.125 alloys, respectively. Increasing tendency of the incomplete MPT with x is clearly visible in the phase fraction plots. Notably, increasing austenite phase fraction below the MPT results in a decrease in T_M. Our refinement analysis also confirms the monotonic increase of the hexagonal and orthorhombic lattice parameters with increasing sample T. This behavior matches well with the previously reported doped MnNiGe alloys having no vacancies [29,30]. The variation of lattice parameters is shown in Fig. S1 of the Supplemental Materials [33].

B. Dc magnetic measurements

We recorded T variation of dc magnetization (M) data in the presence of 1 kOe of external H in field cooling (FC) and field-cooled heating (FCH) protocols. These $M(T)$ data are plotted in the main panels of Figs. 3(a) and 3(b) for $x = 0.075$ and 0.125 alloys, respectively. On heating from 5 K, M remains almost unchanged until the T_M of the alloys and beyond that, a sharp increase in the M value has been observed. Further increase in sample T results in a sluggish decrease in the M value up to a certain T (depending on the alloy composition), and after that, a sharp drop in the M value has been observed followed by a slow decrease until 300 K. The observed $M(T)$ behaviors are quite similar to that of the Al/Ga-doped (doping at the Ge site) MnNiGe alloys reported in the literature [15,24–28]. Recent neutron powder diffraction (NPD) study on two such Ge-site-doped alloys confirms the helically modulated incommensurate antiferromagnetic (AFM) martensite → commensurate AFM austenite → paramagnetic (PM) austenite transition during heating from the lowest T of measurements [30]. Similar $M(T)$ behavior indicates the presence of akin magnetic phases in the presently studied alloys. Apart from these characteristic features, an apparent thermal hysteresis between FC and FCH data has also been noticed around the MPT, confirming the first-order nature of the MPT. The T_Ms observed from the magnetization data (175 K and 122 K for alloys with $x = 0.075$ and 0.125, respectively) match well with the transition temperatures obtained from the XRD data. Interestingly, a kinklike feature is found to be visible in the magnetically ordered austenite phase for both the alloys [see insets of Figs. 3(a) and 3(b) for an enlarged view]. Such behavior is quite unique and is only visible for the MEAs having vacancies in both the transition metal sites [14]. To probe the role of any structural change behind such an anomaly, we recorded XRD data with a 5 K interval; however, we did not observe any significant change in the structural parameters (lattice parameters, bond lengths, etc.; see Fig. S1 of the Supplemental Materials [33]) around such transition [kinklike feature in the $M(T)$ data]. This behavior indicates the possible presence of a spin-reorientation transition in the magnetically ordered austenite phase.

To shed more light on the magnetic behavior, we further recorded $M(T)$ data in the presence of higher applied H in FC and FCH protocols. Such high-field $M(T)$ curves are plotted in Figs. 4(a) and 4(b). The behavior of these $M(T)$ curves are found to be significantly different from the pure and doped MEAs having no vacancies. In the low-H region, the magnitude of dc magnetic moment of the magnetically ordered austenite phase was found to be greater than the moment values of the martensite phase. However, with the increasing value of the external H, the moment value of the martensite phase starts to increase, and eventually, the magnetic moment of the martensite phase becomes greater than that of the austenite phase. In the case of foreign-element doping at Ge site of MnNiGe alloys, no such change in the $M(T)$ behavior has been observed with increasing H [15,24–28]. On the other hand, for Mn- and Ni-site-doped alloys, the martensite phase was found to be more magnetic than the austenite phase in both low- and high-H region due to the PM nature of the austenite phase [13,16,17]. Interestingly, no change in the T_M value has been observed in any of the presently studied alloys with increasing H. However, the spin-reorientation transition (kinklike anomaly) observed in the magnetically ordered austenite phase was found to show a strong dependence on the external H, which further confirms the magnetic origin of the observed abnormality in

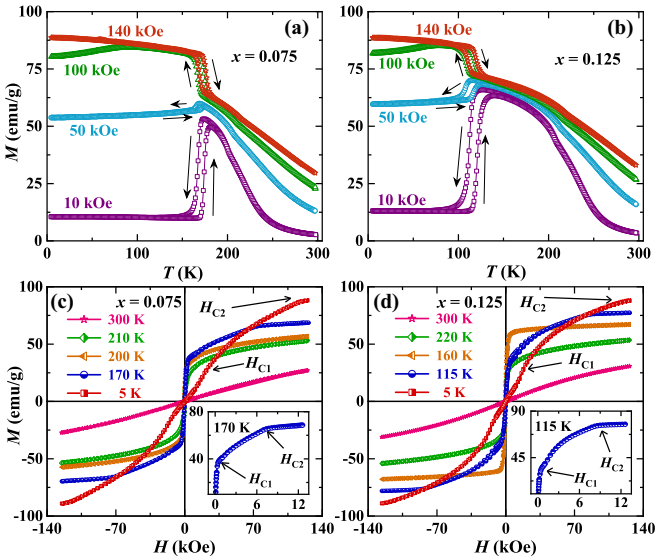

FIG. 4. (a) and (b) depict the dc magnetization M data as a function of temperature T in the presence of 10, 50, 100, and 140 kOe of external magnetic field (H) under field cooling (FC) and field-cooled heating (FCH) protocols for $x = 0.075$ and 0.125 alloys, respectively. Isothermal variation of dc M as a function of H are plotted in (c) and (d) for $x = 0.075$ and 0.125 alloys, respectively. Insets of (c) and (d) depict the enlarged view of the $M(H)$ isotherm, recorded just below the MPT.

the $M(T)$ data. In the presence of 1 kOe of external H, the kinklike feature is found to appear around 200 K and 207 K for $x = 0.075$ and 0.125 alloys, respectively. Such transition temperatures shifted towards higher T and found to appear at 215 K and 220 K for $x = 0.075$ and 0.125 alloys, respectively, in the presence of 140 kOe of external H.

To explore the response of different magnetic phases with external H, we also recorded isothermal variation of M as a function of external H at different constant T. All the $M(H)$ isotherms were recorded in a thermally demagnetized state and are plotted in Figs. 4(c) and 4(d). Such states were obtained by cooling the samples from room T to 5 K (well below the MPT) and heated back to the respective T of measurements in zero magnetic fields. The room T (300 K) isotherms confirm the PM nature of all the studied alloys. On the other hand, the magnetically ordered austenite phase behaves differently [210 and 200 K $M(H)$ isotherms for $x = 0.075$ alloy; 220 and 160 K $M(H)$ isotherms for $x = 0.125$ alloy]. For these $M(H)$ isotherms, initial application of H results in a sharp increase in M, followed by a tendency of partial saturation at higher applied H. The observed behavior is quite similar to that of the Ge-site-doped alloys, indicating a commensurate AFM behavior of the magnetically ordered austenite phase [24], which undergoes a partial field-induced transition to ferromagnetic (FM) phase on application of H, though a significant fraction of AFM phase remains untransformed. Interestingly, below the MPT, an entirely different nature of the $M(H)$ isotherms have been observed [170 and 5 K $M(H)$ isotherms for $x = 0.075$ alloy; 115 and 5 K $M(H)$ isotherms for $x = 0.125$ alloy]. On application of H, the mixture of incommensurate and commensurate AFM phases (due to the incomplete MPT) starts to transform to FM phase, clear from the initial sharp increase in M, followed by a slow increase. Further, an increase in H results in an almost saturating behavior in M. Presence of untransformed commensurate AFM austenite phase prevents complete saturation in the $M(H)$ curve at the low-T region. Two critical fields (during the appearance and completion of the field-induced transition of the majority incommensurate AFM phase) are clearly visible in the isotherms [marked by H_{C1} and H_{C2} in Figs. 4(c) and 4(d)]. Notably, these critical fields show a significant increase with a decrease in sample T [also visible in the $M(H)$ isotherms presented in Fig. S2 of the Supplemental Material [33]]. Observation of a complete field-induced transition to the FM phase from the incommensurate AFM martensitic phase below the MPT is quite unique and has not been observed for any MEAs.

C. Magnetocaloric effect

The presence of a large change in M around the MPT and field-induced metamagnetic transition, both in martensite and magnetically ordered austenite phases, tempted us to calculate the MCE of the presently studied alloys. MCE of a material is defined as the reversible change in the T of the material in a changing H. Isothermal change in magnetic entropy (ΔS) and corresponding adiabatic change in sample T are measures of MCE. Though MCE can be calculated directly from the heat capacity measurements, one can also indirectly calculate it from the dc magnetization data. As per the Maxwell's thermodynamical relation, ΔS of a material in a changing magnetic field ($0 \rightarrow H_0$) can be expressed as $\Delta S(0 \rightarrow H_0) = \int_0^{H_0} (\frac{\partial M}{\partial T})_H dH$ [34]. However, one has to be careful in using Maxwell's relation for MCE calculation around the first-order phase transition, as a discontinuous jump in M will give rise to erratic values of ΔS (due to the infinite value of $(\frac{\partial M}{\partial T})_H$) [35]. Absence of any discontinuity in the $M(H)$ and $M(T)$ data for both the alloys, focused in the present work, allowed us to use Maxwell's relation to calculate the MCE. We recorded several $M(H)$ isotherms (up to 110 kOe of H) with 5 K intervals around the magnetic and martensitic phase transition points and obtained $M(T)$ data at different constant H by convoluting such isotherms. All the $M(H)$ and $M(T)$ data are plotted in the Supplemental Material (Figs. S2 and S3) [33]. The $M(H)$ isotherms were recorded in a thermally demagnetized state to remove any remnant magnetization before measurement. Finally, the convoluted $M(T)$ data were used to calculate ΔS as a function of T. Such $\Delta S(T)$ data obtained for different changing H are plotted in the main panels of Figs. 5(a) and 5(b). Both inverse and conventional MCE behavior have been observed around the MPT and magnetic transitions, respectively. Interestingly, the inverse and the conventional MCE behave very differently with the increase in changing H. With initial increase in H, an increase in the peak value of ΔS around the inverse MCE region has been observed for both the alloys. However, further increase in H beyond the critical field of incommensurate AFM to FM transition in the low-T martensite phase results in a decreasing trend in the peak value of ΔS. Such behavior is unique and possibly the first-ever observation in MEAs. On the other hand, a monotonic increase in the peak values of ΔS

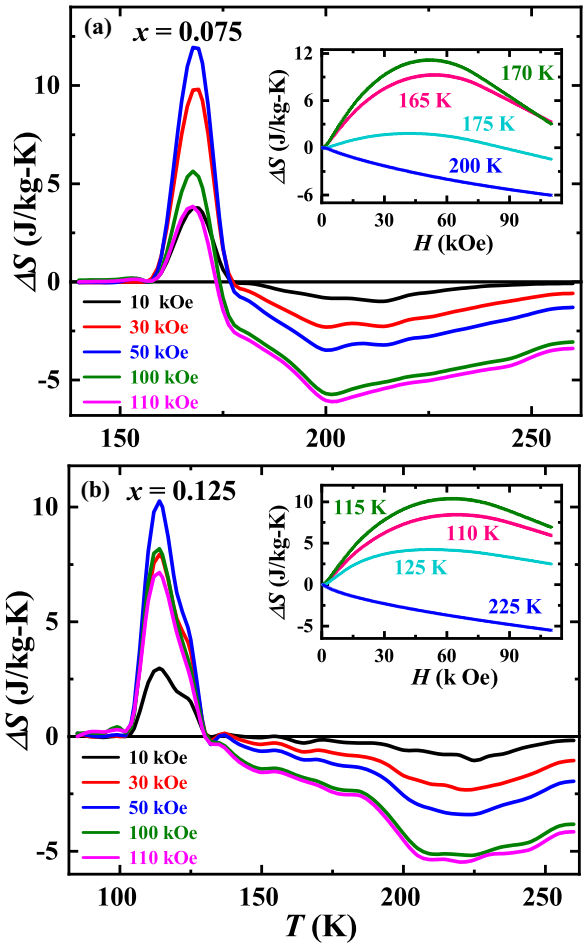

FIG. 5. The main panels of (a) and (b) show the variation of entropy change ΔS as a function of temperature T for different values of changing magnetic fields (H) for $x = 0.075$ and 0.125 alloys, respectively. Insets depict the isothermal variation of ΔS as a function of H at different constant T.

around the conventional MCE region has been observed with increasing changing H. The observed behavior of entropy change ΔS, as a function of H at different constant T (around both inverse and conventional MCE regions), are plotted in the insets of Figs. 5(a) and 5(b). The maximum values of ΔS observed around the inverse MCE are ∼11.14 J/kg-K ($0 \rightarrow 50.9$ kOe; $T = 170$ K), and 10 J/kg-K ($0 \rightarrow 63$ kOe; $T = 115$ K) for $x = 0.075$ and 0.125 alloys, respectively [see insets of Figs. 5(a) and 5(b)]. On the other hand, in the conventional MCE region, the peak values of ΔS for H changing from $0 \rightarrow 110$ kOe are 6.03 J/kg-K and 5.48 J/kg-K for $x = 0.075$ and 0.125 alloys, respectively [see insets of Figs. 5(a) and 5(b)]. The observed magnitudes of ΔS are reasonably large among the members of the MEA family. Refrigeration capacity (RC), defined as $\mathrm{RC} = \int_{T_{\mathrm{cold}}}^{T_{\mathrm{hot}}} \Delta S(T)\mathrm{d}T$, is an important parameter of a material, which indicates the applicability of the material as a magnetic refrigerant [36]. Here, T_{hot} and T_{cold} are source and sink temperatures, respectively. In the inverse MCE region, the RC values of $x = 0.075$ and 0.125 alloys came out to be 92 and 118 J-kg^{-1}, respectively, for 50 kOe of H change. On the other hand, about 366 and 398 J-kg^{-1} of RC values have been observed for 110 kOe of change in H around the conventional MCE region for $x = 0.075$ and 0.125 alloys, respectively. The observed values of RC are reasonably high among MEAs.

IV. DISCUSSION AND CONCLUSIONS

Co-doped $MnNiGe_{1.05}$ alloys having significant amounts of vacancies, both at Mn and Ni sites, with nominal compositions $MnNi_{1-x}Co_xGe_{1.05}$ (for $x = 0.075$, 0.125) were investigated through T-dependent XRD and dc magnetization study. Incomplete MPT, field-induced transition in the low-T martensite phase, the possible presence of spin-reorientation transition in the magnetically ordered austenite phase, and inverse and conventional MCE are some of the unique features unveiled in the present study. Though some previous reports indicate the presence of incomplete MPT in the foreign-element-doped alloys, having no vacancy in any of the transition-metal sites, the observed phase fraction of the high-T hexagonal phase below T_M was generally <15% [13,29,30]. However, for the presently studied alloys, the observed percentages of the high-T austenite phase at the lowest T of measurement is quite high. For $x = 0.125$ alloy, about 35.02% of high-T austenite phase has been noticed at 25 K. Such observation indicates that increasing Co doping in the presence of vacancy at the transition-metal sites prefers high-T austenite phase. Notably, a decrease in lattice parameters has been noticed with increasing Co concentration (see Table I). Such behavior confirms the generation of positive chemical pressure in the system with Co doping (through the decrease of lattice parameters and hence lattice volume). Interestingly, recent neutron powder diffraction in the presence of external pressure revealed that the application of pressure induces incomplete MPT in the Fe-doped MnNiGe alloys [29]. This confirms the role of increasing chemical pressure behind the observed increase in the incomplete MPT with increasing Co concentration.

The existence of a significant amount of magnetically ordered (commensurate AFM) austenite phase well below the MPT results in a remarkable effect on the magnetic behavior of the low-T martensite phase. Depending on the strength of the external H, the moment value of the martensite phase was found to be less or greater than the moment values of the austenite phase. No such observation has previously been reported in any of the existing pure or doped alloys of the MEA family. The presence of field-induced AFM (commensurate as well as incommensurate) to FM transition is mainly responsible for such observation. Incomplete MPT and hence the existence of a large fraction of high-T austenite phase in the low-T region triggered such field-induced transition and unique magnetic properties. Field-induced transitions in both alloys were further confirmed from the $M(H)$ isotherms. Notably, the critical fields for the field-induced transition below the MPT region depend strongly on the sample temperature. A significant increase in the critical field values has been observed with decreasing sample temperature.

Apart from the unique magnetic behavior of the low-T martensite phase, the kinklike feature observed in the magnetically ordered austenite phase is exclusive for the presently studied Co-doped alloy family having vacancy

at the transition metal sites. The absence of any structural distortions/modifications around the kinklike feature, confirmed from the T-dependent XRD data, suggested the magnetic origin of the observed anomaly in the austenite phase. Similar oddity observed in T-dependent magnetization data at the martensite phase of pure and Fe-doped MnNiGe alloys was identified to be a spin-reorientation transition through neutron powder diffraction study [29]. Resemblance of the irregular feature in the $M(T)$ data indicated the possible presence of spin-reorientation transition in the magnetically ordered austenite phase in the presently studied alloys.

An interesting feature has also been found to be associated with magnetocaloric properties. Observing both conventional and inverse magnetocaloric effects is not uncommon for pure and doped MEAs [13–21,26–28]. However, the presence of a significant amount of high-T austenite phase well below the MPT and field-induced transitions triggered a new aspect in the inverse MCE region. The change in magnetic entropy ΔS was found to show a nonmonotonic behavior with external H in the inverse MCE region. With the initial application of H, the low-T phase undergoes field-induced transition, which results in an increase in disorder in the system and, hence, an increase in ΔS values has been observed, as entropy is a measure of disorder. The ΔS becomes maximum when the disorder in the low-T phase becomes maximum (when the moment values of low- and high-T phases become equal). On further increase in applied H, most of the low-T phase becomes FM and, hence, an ordered phase has been achieved. This results in a decrease in ΔS.

In conclusion, the present work, based on the structural and magnetic investigations of the Co-doped $MnNiGe_{1.05}$ alloys (having vacancies at the transition metal sites) reveal the role of incomplete MPT on the magnetic and magnetofunctional properties. The presence of both commensurate AFM (austenite) and incommensurate AFM (martensite) phases triggered a smooth path for the field-induced transition to the FM phase. Such field-induced transition results in a nonmonotonic change in the MCE behavior. The possible presence of a spin-reorientation transition in the austenite phase is another important outcome of the present work. However, detailed microscopic studies (e.g., neutron powder diffraction) are essential to confirm the presence of any spin-reorientation transition. The presently studied alloys are a good addition to the existing family of MEAs from fundamental as well as from application point of view.

ACKNOWLEDGMENTS

S.C. and R.R. would like to thank the Science and Engineering Research Board (SERB), DST-India, for financial support (Project No. CRG/2020/000670). Portions of this research were carried out at the light source PETRA-III electron storage ring at DESY (Proposal No. I-20220954), a member of the Helmholtz Association (HGF). Financial support by the Department of Science and Technology (Government of India) provided within the framework of the India@DESY collaboration is gratefully acknowledged.

[1] Y. Sutou, Y. Imano, N. Koeda, T. Omori, R. Kainuma, K. Ishida, and K. Oikawa, Appl. Phys. Lett. **85**, 4358 (2004).
[2] R. Kainuma, Y. Imano, W. Ito, Y. Sutou, H. Morito, S. Okamoto, O. Kitakami, K. Oikawa, A. Fujita, T. Kanomata, and K. Ishida, Nature (London) **439**, 957 (2006).
[3] V. K. Sharma, M. K. Chattopadhyay, K. H. B. Shaeb, A. Chouhan, and S. B. Roy, Appl. Phys. Lett. **89**, 222509 (2006).
[4] T. Krenke, E. Duman, M. Acet, E. F. Wassermann, X. Moya, L. Mañosa, and A. Planes, Nat. Mater. **4**, 450 (2005).
[5] S. Y. Yu, Z. H. Liu, G. D. Liu, J. L. Chen, Z. X. Cao, G. H. Wu, B. Zhang, and X. X. Zhang, Appl. Phys. Lett. **89**, 162503 (2006).
[6] M. Khan, I. Dubenko, S. Stadler, and N. Ali, Appl. Phys. Lett. **91**, 072510 (2007).
[7] S. Chatterjee, S. Giri, S. Majumdar, and S. K. De, Phys. Rev. B **77**, 012404 (2008).
[8] S. Chatterjee, S. Giri, S. Majumdar, and S. K. De, Phys. Rev. B **77**, 224440 (2008).
[9] S. Chatterjee, S. Giri, S. K. De, and S. Majumdar, Phys. Rev. B **79**, 092410 (2009).
[10] S. Chatterjee, S. Giri, S. K. De, and S. Majumdar, Phys. Rev. B **81**, 214441 (2010).
[11] K. Koyama, M. Sakai, T. Kanomata, and K. Watanabe, Jpn. J. Appl. Phys. **43**, 8036 (2004).
[12] W. Bazela, A. Szytuła, J. Todorović, Z. Tomkowicz, and A. Zięba, Physica Stat. Sol. (a) **38**, 721 (1976).
[13] E. Liu, W. Wang, L. Feng, W. Zhu, G. Li, J. Chen, H. Zhang, G. Wu, C. Jiang, H. Xu, and F. de Boer, Nat. Commun. **3**, 873 (2012).
[14] C. Zhang, D. Wang, Q. Cao, S. Ma, H. Xuan, and Y. Du, J. Phys. D: Appl. Phys. **43**, 205003 (2010).
[15] T. Samanta, I. Dubenko, A. Quetz, S. Temple, S. Stadler, and N. Ali, Appl. Phys. Lett. **100**, 052404 (2012).
[16] P. Dutta, S. Pramanick, S. Majumdar, D. Das, and S. Chatterjee, J. Magn. Magn. Mater. **395**, 312 (2015).
[17] K. Mandal, S. C. Das, P. Dutta, S. Pramanick, and S. Chatterjee, J. Alloys Compd. **822**, 153454 (2020).
[18] C. L. Zhang, D. H. Wang, Q. Q. Cao, Z. D. Han, H. C. Xuan, and Y. W. Du, Appl. Phys. Lett. **93**, 122505 (2008).
[19] N. T. Trung, L. Zhang, L. Caron, K. H. J. Buschow, and E. Brück, Appl. Phys. Lett. **96**, 172504 (2010).
[20] L. Caron, N. T. Trung, and E. Brück, Phys. Rev. B **84**, 020414(R) (2011).
[21] I. Dincer, E. Yüzüak, G. Durak, Y. Elerman, A. M. T. Bell, and H. Ehrenberg, J. Alloys Compd. **540**, 236 (2012).
[22] N. T. Trung, V. Biharie, L. Zhang, L. Caron, K. H. J. Buschow, and E. Brück, Appl. Phys. Lett. **96**, 162507 (2010).

[23] J. Wang, D. Wang, C. Chen, O. Nashima, T. Kanomata, H. Mizuseki, and Y. Kawazoe, Appl. Phys. Lett. **89**, 262504 (2006).
[24] P. Dutta, D. Das, S. Chatterjee, S. Pramanick, and S. Majumdar, J. Phys. D: Appl. Phys. **49**, 125001 (2016).
[25] K. Mandal, S. Das, P. Dutta, S. Pramanick, and S. Chatterjee, J. Magn. Magn. Mater. **552**, 169177 (2022).
[26] A. Quetz, T. Samanta, I. Dubenko, M. J. Kangas, J. Y. Chan, S. Stadler, and N. Ali, J. Appl. Phys. **114**, 153909 (2013).
[27] C. L. Zhang, Z. D. Han, B. Qian, H. F. Shi, C. Zhu, J. Chen, and T. Z. Wang, J. Appl. Phys. **114**, 153907 (2013).
[28] E. Liu, Y. Du, J. Chen, W. Wang, H. Zhang, and G. Wu, IEEE Trans. Magn. **47**, 4041 (2011).
[29] R. Roy, S. K. Adhikari, J. Sannigrahi, K. Mandal, S. C. Das, P. Dutta, S. Pramanick, D. Khalyavin, D. T. Adroja, and S. Chatterjee, Phys. Rev. B **104**, 214405 (2021).
[30] S. C. Das, J. Sannigrahi, P. Dutta, S. Pramanick, D. Khalyavin, D. T. Adroja, and S. Chatterjee, Phys. Rev. B **103**, 094422 (2021).
[31] J. Rodríguez-Carvajal, Phys. B: Condens. Matter **192**, 55 (1993).
[32] K. Momma and F. Izumi, J. Appl. Cryst. **44**, 1272 (2011).
[33] See Supplemental Material at http://link.aps.org/supplemental/10.1103/PhysRevB.109.144420 for (i) temperature variation of the lattice parameters; (ii) isothermal M(H) data recorded at different constant temperatures for MCE calculation; (iii) convoluted M(T) curves obtained from the M(H) isotherms.
[34] V. K. Pecharsky and K. A. Gschneidner Jr, J. Magn. Magn. Mater. **200**, 44 (1999).
[35] N. A. de Oliveira and P. J. von Ranke, Phys. Rev. B **77**, 214439 (2008).
[36] K. A. Gschneidner Jr, V. K. Pecharsky, and A. O. Tsokol, Rep. Prog. Phys. **68**, 1479 (2005).